Douglas, John and Aochi, Hideo (2016) Assessing components of ground-motion variability from simulations for the Marmara Sea region (Turkey). Bulletin of the Seismological Society of America, 106 (1). pp. 300-306. ISSN 0037-1106 , http://dx.doi.org/10.1785/0120150177

Assessing components of ground-motion variability from simulations for the Marmara Sea region (Turkey)

John Douglas* and Hideo Aochi

* Address of corresponding author

University of Strathclyde

Department of Civil and Environmental Engineering

Level 5

James Weir Building

75 Montrose Street

G1 1XJ

Scotland

United Kingdom

Tel: +44 (0)141 548 4569

email: john.douglas@strath.ac.uk

Submitted to the Bulletin of the Seismological Society of America

Originally submitted: July 6 2015

Resubmitted: September 23 2015

Accepted: October 4 2015

Abstract

Recent studies have shown that repeatable travel-path terms make a high contribution to the overall variability in earthquake ground motions. Having maps of such terms available for a given recording site would, theoretically, allow removal of this component from the aleatory variability of ground-motion models. The assessment of such travel path terms for a given site, however, relies on having recorded a rich set of earthquakes at that site. Given the relative youth of strong-motion networks the assessment of such terms from observations is currently difficult for most parts of the world. Ground-motion simulations, however, provide an alternative method to assess such terms.

In this article many dozens of earthquakes, distributed in a grid, are simulated for the Marmara Sea region (Turkey), which borders the megacity of Istanbul and is an area of high seismic hazard. Ground motions are simulated within a detailed 3D velocity structure model using a finite-difference method at 70 recording sites in the area (200×120 km). Horizontal peak ground velocities from these simulations are regressed to derive a ground-motion model. Next, residuals from these GMPEs are computed to assess repeatable source, site and path terms and various components of ground-motion variability. These components are similar to those derived from real strong-motion data, thereby lending support to those estimates as well as showing the worth of simulations for this type of exercise.

Introduction

Ground motion prediction equations (GMPEs) provide a means of estimating the median earthquake ground motion, in terms of a scalar intensity measure (IM), and its aleatory variability, commonly called sigma (σ). IMs include parameters such as peak ground acceleration and velocity (PGA and PGV) and elastic response spectral accelerations. Many hundreds of GMPEs have been published in the past fifty years (Ground motion prediction equations 1964-2015, see Data and Resources). Until relatively recently σ has been less well studied than other aspects of these models. In the past decade, however, numerous studies on σ and its various components have been published (Strasser et al, 2009; Al Atik et al, 2010). It is now common to split ground-motion variability into the part associated with the earthquake (between-event) (Joyner and Boore, 1981, 1993) and the within-event remainder. In addition, there have been an increasing number of studies that also evaluate the between-site component (Joyner and Boore, 1993; Chen and Tsai, 2002). The remaining component of variability that has not been commonly estimated is the between-path portion.

The reason why path terms are important for seismic hazard assessments is that, theoretically, they could be included within these assessments (e.g. through a map of the terms for a given site) and the total σ within these evaluations reduced. This is similar to the situation when a site term is known and the σ used should be the single-station σ (Atkinson, 2006).

To evaluate robust travel-path terms (and consequently between-path variability) requires travel-paths that have been roughly repeated many times, which means that a dense strong-motion network that has recorded many earthquakes is necessary. This requirement meant that such calculations were not possible using observational data until the advent of dense digital networks in highly-seismically active regions, e.g. TriNet in California and K-Net and KiK-net in Japan. Based on data from such networks a handful of studies have been conducted to extract the repeatable path component of earthquake ground motions.

The first such study was by Atkinson (2006) using data from California. She evaluated the reduction in σ when considering a single site and also a single path-single site by using sets of earthquakes in small geographical zones (i.e. sampling roughly the same travel-paths). A large reduction (40%) in σ was found for the case of single path-single site. Morikawa et al (2008) used Japanese earthquakes from small areas recorded at the same stations and found that σ was lower, and of a similar order to that found by Atkinson (2006), than when data with many travel-paths were used. An extension of this approach was applied by Anderson and Uchiyama (2011) to data from Japan and Guerrero (Mexico) and they found large reductions in the σ (e.g. from 0.64 to 0.40 in terms of $\ln \mathrm{PGV}$) after applying path corrections. A more sophisticated method was used by Dawood and Rodriguez-Marek (2013) to analyze strong-motion data from aftershocks of the 2011 Tohoku (Japan) earthquake. They provide a map of regional anelastic attenuation terms and the residual σ when these terms are used. Again a significant reduction in σ was identified. The study by Lin et al (2011), using Taiwanese data, differs from the others because it does not rely on grouping earthquakes and stations into small geographical regions for which repeated travel-path terms can be estimated. The method is based on a closeness index (CI) that measures, for each station, how similar the travel-paths are for pairs of earthquakes (null means that they are the same and two means that they are diametrically opposite). By using CI they evaluate the reduction in σ, which was found to be of a similar order to the reductions reported by Atkinson (2006) and Morikawa et al (2008).

These studies are all based on observational data, which have limitations in terms of the geographical density of the earthquakes and stations and the number of (near) repeated travel-paths. In addition, the earthquake and site characteristics of the data used are heterogeneous and uncertain, which could affect the components of σ evaluated. Ground-motion simulations have the advantage of allowing as many earthquake-site pairs as required to be created and, for all of these, the exact meta-data (e.g. locations and magnitudes) be controlled and known. This means that more robust estimates of the event, site and path terms and, subsequently, the different components of variability should be able to be computed, as recently discussed for large earthquakes in southern California (Wang and Jordan, 2014; Villani and Abrahamson, 2015).

The aim of this Short Note is to evaluate the various components of ground-motion variability using a set of simulations for the Marmara Sea region (Turkey). This region has been chosen as it is an area of high seismic hazard and risk and consequently the results obtained could help guide future studies in this region. In addition, the velocity structure in this region is well constrained and ground-motion simulations have been calibrated previously.

The next section summarizes the ground-motion simulations used for this study. The subsequent section presents the results of the analysis of these simulations to estimate the various components of variability. The article ends with a comparison with previous results and a summary of the principal findings.

Simulations

We focus on a region centered on the Marmara Sea (Turkey) with dimensions of $200\,(\mathrm{EW}) \times 120\,(\mathrm{NS}) \times 40\,(\mathrm{depth})\ \mathrm{km}^3$, in which 70 receivers (based on the seismic network in this region) are distributed. The crustal structure model (Figure 1(top)) (Aochi and Ulrich, 2015) is constructed by combining 3D tomography (Bayrakci et al, 2013), bathymetry from the General Bathymetric Chart of the Oceans and a regional 1D-layered model (Figure 1(bottom), H. Karabulut, written communication). The Marmara Sea is included as a water layer (shear velocity $V_s = 0\,\mathrm{km/s}$). The 3D calculation of the ground motions are made using a 3D finite difference method (Aochi and Madariaga, 2003; Aochi et al, 2011) that is fourth-order in space and second-order in time on staggered grids. The minimum wave velocity is the P-wave ($V_p = 1.5\,\mathrm{km/s}$)

velocity in the water layer. We use a grid size of $\Delta s = 200\,\mathrm{m}$. Hence, the maximum frequency of the calculations is at least $V_{min}/(5\Delta s) = 1.5\,\mathrm{Hz}$. The maximum velocity in the model is $7.94\,\mathrm{km/s}$. Therefore, a time step of the finite difference should be less than $(5\Delta s)/V_{max} = 0.0126\,\mathrm{s}$ for the purposes of stability; hence, we use a time-step of $0.01\,\mathrm{s}$. Each calculation is run for 12000 time steps, i.e. $120\,\mathrm{s}$. The outer boundary, except for the free surface, is surrounded by a perfectly-matched-layer absorbing zone to avoid efficiently any artificial reflections (Collino and Tsogka, 2001).

Any kinematic source can be introduced by a temporally-variable seismic moment release function. A finite source could be modeled as a series of point sources (Aochi et al, 2013). For the purpose of this study, we use a point source of magnitude $M_w 5$ for each simulation by assuming a source time function from a B-spline with a duration of $1.3\,\mathrm{s}$ (Douglas et al, 2007), which assumes a fault dimension of $3\,\mathrm{km}$ and a rupture velocity of $2.2\,\mathrm{km/s}$ (Figure 2). 39 point sources are uniformly distributed over the region at a focal depth of $7\,\mathrm{km}$ and another 39 at a depth of $12\,\mathrm{km}$; this is consistent with the observed depths in the Marmara Sea. A uniform distribution of earthquakes is preferred over one that matched the observed seismicity to make visualization of the event terms easier and to ensure a good distribution of source-to-site distances. The fault mechanisms of the sources are (strike, dip, rake): $(0^\circ, 90^\circ, 180^\circ)$ (pure strike-slip) and $(130^\circ, 63^\circ, -63^\circ)$ (oblique normal), which are the predominant mechanisms in this region. In total, $4 \times 39 = 156$ simulations are carried out, which leads to $70 \times 156 = 10\,920$ ground-motion time histories. From these we extract the geometric mean of the PGV of the two horizontal components. This IM was chosen as it should not be strongly affected by the relatively low maximum frequency of the simulations and because previous estimates of ground-motion variability from observational data have been reported for PGV.

Results

The procedure followed to compute the different components of variability follows closely Lin et al (2011), to which the interested reader is referred for details of the approach. Here only the principal results are reported.

Ground-motion model

The analysis is based on residuals with respect to a GMPE. Lin et al (2011) adjusted the GMPE of Chiou and Youngs (2008) using mixed-effects regression to make it more applicable to the Taiwanese data that they used. As all of the simulations conducted for this study are for point sources of a single magnitude ($M_w 5$), this simple functional form is used for the GMPE here:

$$\ln \mathrm{PGV} = a_1 + a_2 \ln[\min(R, R_0)] + a_3 \ln\{\min[\max(R, R_0), R_1]\} + a_4 \ln[\max(R, R_1)], \tag{1}$$

where a_1 to a_4 are found by regression and R is hypocentral distance. This trilinear function was chosen based on visual inspection of the simulated PGVs and, using trial-and-error, R_0 and R_1 were set to 110 and 150 km, respectively. The increase in PGV beyond R_0 is due to reflections off the Moho discontinuity. Other functional forms would probably fit the data as well but this should not strongly affect the results obtained. Because all stations recorded all earthquakes, standard least-squares regression can be used rather than mixed-effect analysis, which simplifies the calculations. The simulated PGVs for the four sets of earthquakes and the best-fit curve are shown in Figure 3. It can be seen that the GMPE fits the data well at all distances. Also the PGVs from the four sets of events are similar. Also plotted on Figure 3 are predicted PGVs from the recent GMPE of Bindi et al (2014) derived using data from Turkey and elsewhere in Europe and the Middle East. Predictions from this model match the simulated PGVs closely, demonstrating that the simulations are realistic.

Various components of variability are reported in Table 1. These were computed using the average event and site terms and then by correcting the total residuals by these terms. This is similar to Stages I to IV of Anderson and Uchiyama (2011). These calculations are discussed next.

Maps of event, site and path terms

The event terms are shown in Figure 4. For all sets of sources the event terms around the edge of the Marmara Sea are generally positive, indicating larger than average PGVs, whereas those underneath the Sea produce on average lower PGVs (negative event terms). The ground motions from the strike-slip sources (left maps) are generally more variable than those from the normal sources (right maps). Site terms (Figure 5) indicate higher than average PGVs on the islands within the Marmara Sea. Path terms are difficult to plot because they concern all points along the travel path between event and site. They are plotted as a point (10 920 in all) at a random distance along the travel path between source and station to reduce overlaps and to give an indication of the spatial variability of these terms (Figure 6). No clear patterns in the path terms are visible, which suggests that the ϕ_{SS} component of the variability cannot be reduced easily.

Path and source-location components of variability

The approach developed by Lin et al (2011) using CI, $\Delta\xi_{r_{ijk}}$ and $\Delta\eta_{i,j}$ is applied to compute the path and source-location components of variability. These variables are defined thus:

$$\begin{aligned} \mathrm{CI}_{ijk} &= \frac{\Delta H_{ij}}{(R_{ik}+R_{jk})/2}, && (2)\\ \Delta\xi_{r_{ijk}} &= \frac{\xi_{r_{ik}}-\xi_{r_{jk}}}{\sqrt{2}\phi_{SS}}, && (3)\\ \Delta\eta_{ij} &= \frac{\eta_{E_i}-\eta_{E_j}}{\sqrt{2}\tau}, && (4) \end{aligned}$$

where ΔH_{ij} is the distance between the ith and jth hypocentres, R_{ik} is the hypocentral distance between the ith earthquake and kth site, ξ_r are normalized residuals after correcting for the site terms and η_E are event terms.

As expected, CI and $\Delta\xi_r^2$ are positively correlated because ground motions at close stations are more similar than those from distant stations. The result of averaging the $\Delta\xi_r^2$ estimates in twenty linearly-spaced intervals and computing the standard deviation ($\sigma_{\Delta\xi_r}$) is shown in Figure 7. It was not possible to constrain all coefficients in the complex parametrization of Lin et al (2011) of this variable. Consequently a simple linear function was fit, which is shown in Figure 7. After removing the normalization, the path-to-path and the residual standard deviations are those given in Table 1.

Following a similar procedure, the relationship between event-separation distance and $\Delta\eta^2$ is computed. After computing the average in twenty distance bins and converting to the standard deviation ($\sigma_{\Delta\eta}$) a weak dependence of variability on event-separation distance is found, as expected (Figure 8). Again the nonlinear function used by Lin et al (2011) was not justified given the scatter in $\sigma_{\Delta\eta}$. Consequently a straight line was fit, as shown in Figure 8. After removing the normalization, the location-to-location and the residual standard deviations are obtained (Table 1). Also reported in Table 1 are single-station and single-station-single-path σ computed using the various components.

Discussion and conclusions

Because no variability was introduced into the seismic moment release function used for the simulations the value of τ, expressing the between-event variability, is lower than has been reported in empirical studies. Similarly the within-event component and its subcomponents are lower than obtained from analysis of real strong-motion data. This is probably due to the lack of near-surface variations in the velocity model and because scattering was not included. This is a limitation of this study. Nevertheless the relationships between the different components roughly match empirical estimates. For example, $\sigma_{SS} = 0.89\sigma_T$ and $\sigma_{SP} = 0.77\sigma_T$, which compare favorably, although they are slightly higher, than those reported for a response spectral acceleration of 1 s using this as a proxy for PGV (the period dependence of these relations is weak so a choice of a different proxy period will not change the conclusions): $\sigma_{SS} = 0.87\sigma_T$ (Lin et al, 2011) and $\sigma_{SS} = 0.92\sigma_T$ (Atkinson, 2006); and $\sigma_{SP} = 0.58\sigma_T$ (Lin et al, 2011), $\sigma_{SP} = 0.67\sigma_T$ (Atkinson, 2006) and $\sigma_{SP} = 0.47\sigma_T$ (Morikawa et al, 2008).

Our simulations suggest that the Marmara Sea's geometry leads to earthquakes near its edges generating higher than average ground motions. Also it is found that islands in the Sea are prone to higher than average shaking. Both these findings merit being validated by observational studies given the masses of ground-motion data now being routinely recorded and the high seismic risk in this region.

This analysis demonstrates that the ground-motion simulations show similar characteristics in terms of variability due to path to those observed in real data. Therefore, they provide a means of improving our understanding of ground-motion variability. Based on this improved understanding, appropriate variability components can be used within seismic hazard assessments for engineering purposes, thereby limiting possible 'double counting'.

Data and resources

No observational data were used for this article. The simulations are available upon request from the authors. A compendium of published ground-motion models was obtained from the website `www.gmpe.org.uk`, last accessed October 2015.

Acknowledgments

This study was partially supported by MARsite (New Directions in Seismic Hazard Assessment through Focused Earth Observation in the Marmara Supersite), which received funding from the European Commission's Seventh Framework Programme under grant agreement number 308417. The numerical simulations are carried out at the French National Supercomputing Center 'Grand Equipement National de Calcul Intensif/Centre Informatique National de l'Enseignement Supérieur' under grant number 46700. We thank two anonymous reviewers for their comments on an earlier version of this study.

References

Al Atik L, Abrahamson N, Bommer JJ, Scherbaum F, Cotton F, Kuehn N (2010) The variability of ground-motion prediction models and its components. Seismological Research Letters 81(5):794–801, DOI 10.1785/gssrl.81.5.794

Anderson JG, Uchiyama Y (2011) A methodology to improve ground-motion prediction equations by including path corrections. Bulletin of the Seismological Society of America 101(4):1822–1846, DOI 10.1785/0120090359

Aochi H, Madariaga R (2003) The 1999 Izmit, Turkey, earthquake: Nonplanar fault structure, dynamic rupture process, and strong ground motion. Bulletin of the Seismological Society of America 93(3):1249–1266

Aochi H, Ulrich T (2015) A probable earthquake scenario near Istanbul determined from dynamic simulations. Bulletin of the Seismological Society of America 105(3):1468–1475 DOI 10.1785/0120140283

Aochi H, Durand V, Douglas J (2011) Influence of super-shear earthquake rupture models on simulated near-source ground motion from the 1999 Izmit, Turkey, earthquake. Bulletin of the Seismological Society of America 101(2):726–741, DOI 10.1785/0120100170

Aochi H, Ulrich T, Ducellier A, Dupros F, Michea D (2013) Finite difference simulations of seismic wave propagation for understanding earthquake physics and predicting ground motions: Advances and challenges. Journal of Physics: Conference Series 454(012010), DOI 10.1088/1742-6596/454/1/012010

Atkinson GM (2006) Single-station sigma. Bulletin of the Seismological Society of America 96(2):446–455, DOI 10.1785/0120050137

Bayrakci G, Ligle M, Bécel A, Hirn A, Taymaz T, Yolsal-Çevikbilen S and SEISMARMARA team (2013) 3-D sediment-basement tomography of the Northern Marmara trough by a dense OBS network at the nodes of a grid of controlled source profiles along the North Anatolian fault. Geophysical Journal International 194:1335–1357, DOI 10.1093/gji/ggt211

Bindi D, Massa M, Luzi L, Ameri G, Pacor F, Puglia R, Augliera P (2014) Pan-European ground-motion prediction equations for the average horizontal component of PGA, PGV, and 5%-damped PSA at spectral periods up to 3.0 s using the RESORCE dataset. Bulletin of Earthquake Engineering 12(1):391–430, DOI 10.1007/s10518-013-9525-5

Chen YH, Tsai CCP (2002) A new method for estimation of the attenuation relationship with variance components. Bulletin of the Seismological Society of America 92(5):1984–1991

Chiou BSJ, Youngs RR (2008) An NGA model for the average horizontal component of peak ground motion and response spectra. Earthquake Spectra 24(1):173–215, DOI 10.1193/1.2894832

Collino F, Tsogka C (2001) Application of the perfectly matched absorbing layer model to the linear elastodynamic problem in anisotropic heterogeneous media. Geophysics 66:294–307

Dawood HM, Rodriguez-Marek A (2013) A method for including path effects in ground-motion prediction equations: An example using the M_w9.0 Tohoku earthquake aftershocks. Bulletin of the Seismological Society of America 103(2B):1360–1372, DOI 10.1785/0120120125

Douglas J, Aochi H, Suhadolc P, Costa G (2007) The importance of crustal structure in explaining the observed uncertainties in ground motion estimation. Bulletin of Earthquake Engineering 5(1):17–26, DOI 10.1007/s10518-006-9017-y

Joyner WB, Boore DM (1981) Peak horizontal acceleration and velocity from strong-motion records including records from the 1979 Imperial Valley, California, earthquake. Bulletin of the Seismological Society of America 71(6):2011–2038

Joyner WB, Boore DM (1993) Methods for regression analysis of strong-motion data. Bulletin of the Seismological Society of America 83(2):469–487

Lin PS, Chiou B, Abrahamson N, Walling M, Lee CT, Cheng CT (2011) Repeatable source, site, and path effects on the standard deviation for empirical ground-motion prediction models. Bulletin of the Seismological Society of America 101(5):2281–2295, DOI 10.1785/0120090312

Morikawa N, Kanno T, Narita A, Fujiwara H, Okumura T, Fukushima Y, Guerpinar A (2008) Strong motion uncertainty determined from observed records by dense network in Japan. Journal of Seismology 12:529–546, DOI 10.1007/s10950-008-9106-2

Strasser FO, Abrahamson NA, Bommer JJ (2009) Sigma: Issues, insights, and challenges. Seismological Research Letters 80(1):40–56, DOI 10.1785/gssrl.80.1.40

Villani M, Abrahamson NA (2015) Repeatable site and path effects on the ground-motion sigma based on empirical data from southern California and simulated waveforms from the CyberShake platform. Bulletin of the Seismological Society of America, in press, DOI 10.1785/0120140359

Wang F, Jordan TH (2014) Comparison of probabilistic seismic-hazard models using averaging-based factorization. Bulletin of the Seismological Society of America 104(3):1230–1257, DOI 10.1785/0120130263

University of Strathclyde
Department of Civil and Environmental Engineering
Level 5
James Weir Building
75 Montrose Street
G1 1XJ
Scotland
United Kingdom
(J.D.)
Bureau de Recherches Géologiques et Minières (BRGM)
Risks and Prevention Division/Seismic and Volcanic Risks Unit (DRP/RSV)
3 avenue C. Guillemin
BP 36009
45060 Orléans Cedex 2
France
(H.A.)

Table 1: Components of variability based on analysis of simulated PGVs.

Name	Notation of Al Atik et al (2010)	Notation of Lin et al (2011)	Value
Total on soil surface	σ^G	σ_T	0.4177
Between-event	τ	τ_E	0.1281
Within-event	ϕ	σ	0.3976
Site-to-site	ϕ_{S2S}	τ_S	0.1937
Within-event, single-site	ϕ_{SS}	σ_r	0.3472
Residual (after accounting for event, site and path terms)	—	σ_0	0.3003
Path-to-path	ϕ_{P2P}	τ_P	0.2350
Between-events, single-path	τ_0	τ_{E0}	0.1110
Earthquake location-to-location	τ_{L2L}	τ_{SR}	0.0962
Total (for single site)	σ_{SS}	σ_{SS}	0.3701
Total (for single path)	σ^G_{SP}	σ_{SP}	0.3012

All are given in terms of natural logarithms (ln)

List of Figure Captions

1. 3D view of the V_p structure (top) and 1D layered model (V_p and V_s) implemented in the finite difference simulations (bottom).

2. The imposed source time function (seismic moment release rate) for a M_w5 earthquake.

3. Attenuation of PGV with hypocentral distance and the best-fit trilinear (in terms of $\ln R$) curve. Circles are for the strike-slip sources and triangles are for the oblique sources; filled in symbols are for the sources at 7 km and empty symbols are for the sources at 12 km. The coefficients of Equation 1 (dark gray line) obtained are (in terms of m/s): $a_1 = 14.9303$, $a_2 = -1.3853$, $a_3 = 1.7456$ and $a_4 = -4.7933$. Also shown are predicted PGVs from the GMPE of Bindi et al (2014) for a strike-slip source and rock sites (light gray line).

4. Maps of event residuals, where size is proportional to standard deviation, which ranges from 0.2531 to 0.6035. The standard deviations are computed from the residuals from each of the 70 stations that recorded each event. Top maps are for the 7 km sources and bottom maps are for the 12 km sources; left maps are for the strike-slip sources and right maps are for the oblique sources.

5. Map of station residuals, where size is proportional to standard deviation, which ranges from 0.3007 to 0.4459. The standard deviations are computed from the residuals from each of the $4 \times 39 = 156$ events recorded by each station.

6. Map of path residuals. Residual is plotted at a random distance between epicentre and station. Because each event-path-site is only sampled once it is not possible to assess the standard deviation of each residual (unlike for event and site terms).

7. The standard deviation of the normalized residuals ($\sigma_{\Delta\xi_r}$) against closeness index (CI). The equation of the line of best-fit is: $\sigma_{\Delta\xi_r} = 0.8649 + 0.1167\mathrm{CI}$.

8. The standard deviation of the normalized residuals ($\sigma_{\Delta\eta}$) against separation distance (ΔH). The equation of the line of best-fit is: $\sigma_{\Delta\eta} = 0.8665 + 0.0014\Delta H$.

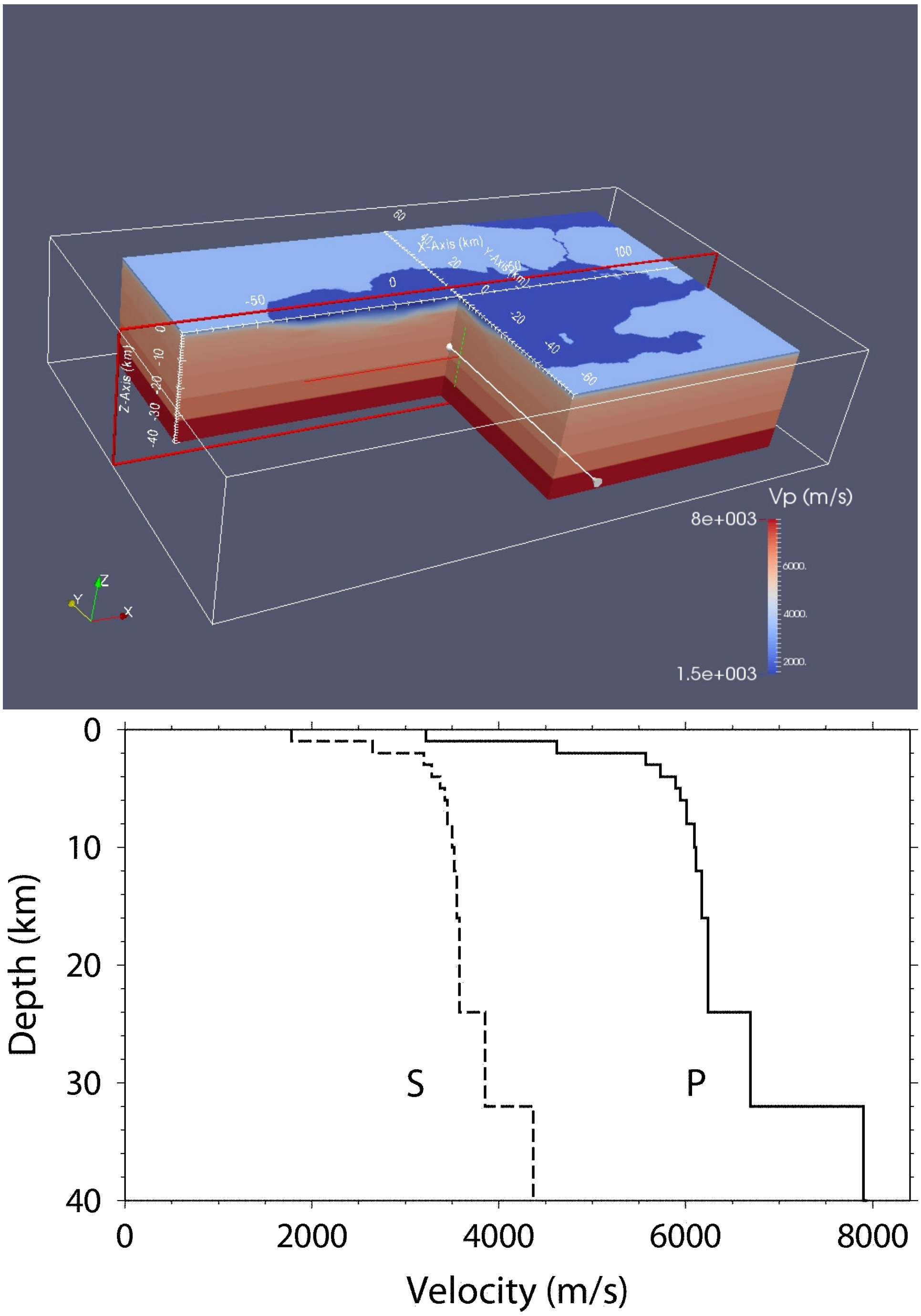

Figure 1: 3D view of the V_p structure (top) and 1D layered model (V_p and V_s) implemented in the finite difference simulations (bottom).

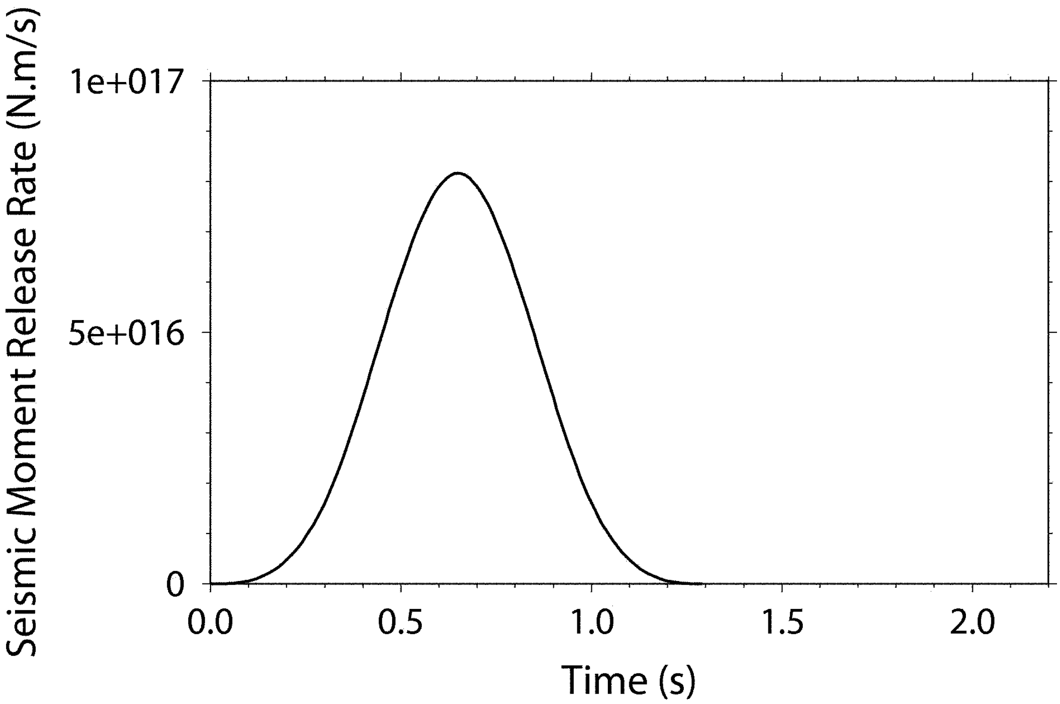

Figure 2: The imposed source time function (seismic moment release rate) for a $M_w 5$ earthquake.

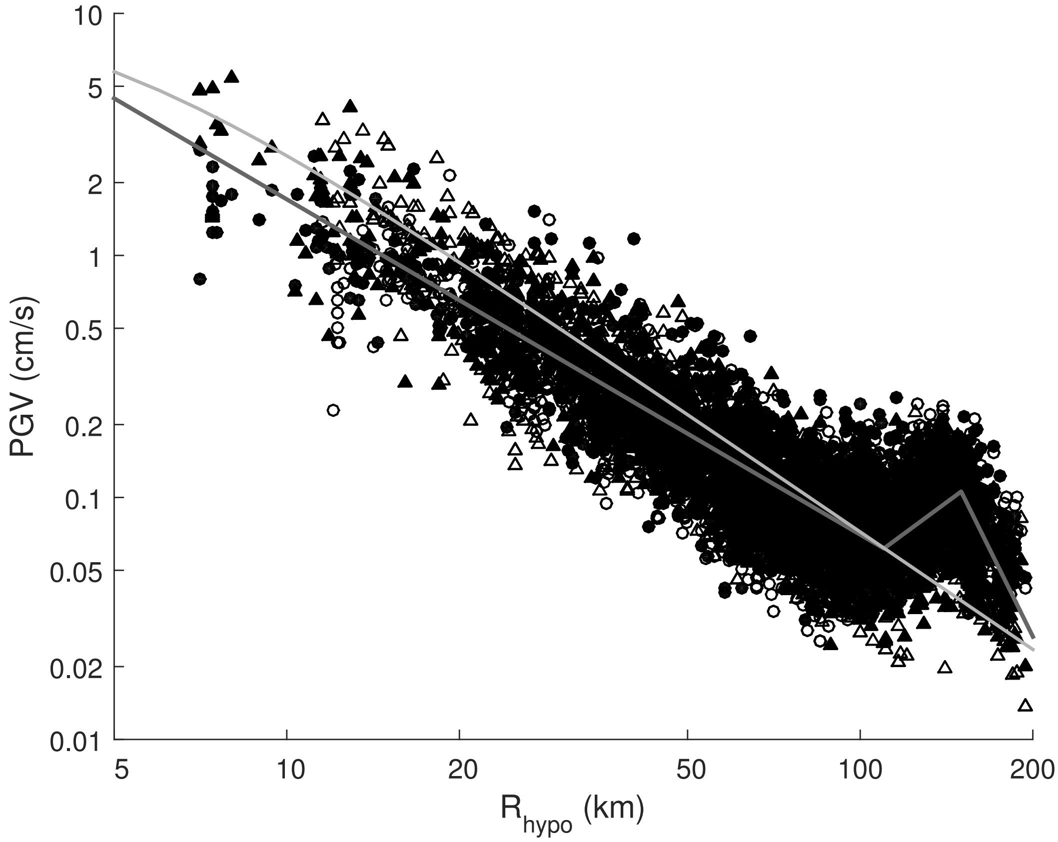

Figure 3: Attenuation of PGV with hypocentral distance and the best-fit trilinear (in terms of $\ln R$) curve. Circles are for the strike-slip sources and triangles are for the oblique sources; filled in symbols are for the sources at 7 km and empty symbols are for the sources at 12 km. The coefficients of Equation 1 (dark gray line) obtained are (in terms of m/s): $a_1 = 14.9303$, $a_2 = -1.3853$, $a_3 = 1.7456$ and $a_4 = -4.7933$. Also shown are predicted PGVs from the GMPE of Bindi et al (2014) for a strike-slip source and rock sites (light gray line).

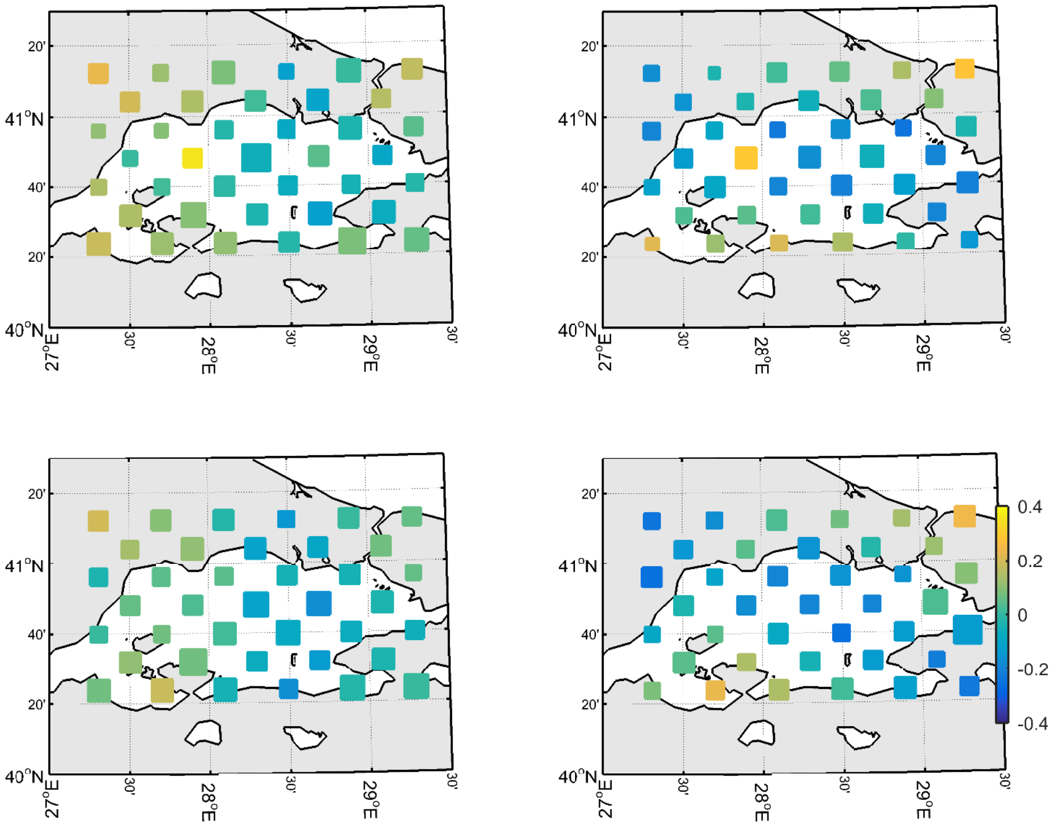

Figure 4: Maps of event residuals, where size is proportional to standard deviation, which ranges from 0.2531 to 0.6035. The standard deviations are computed using the residuals from each of the 70 stations that recorded each event. Top maps are for the 7 km sources and bottom maps are for the 12 km sources; left maps are for the strike-slip sources and right maps are for the oblique sources.

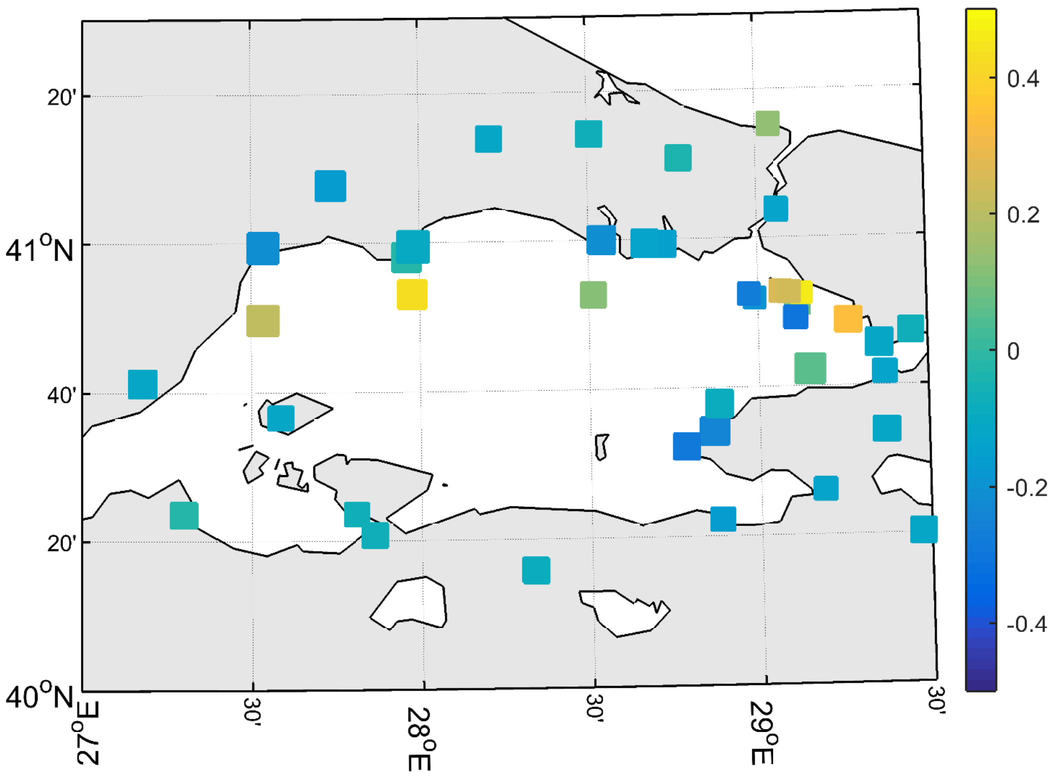

Figure 5: Map of station residuals, where size is proportional to standard deviation, which ranges from 0.3007 to 0.4459. The standard deviations are computed using the residuals from each of the $4 \times 39 = 156$ events recorded by each station.

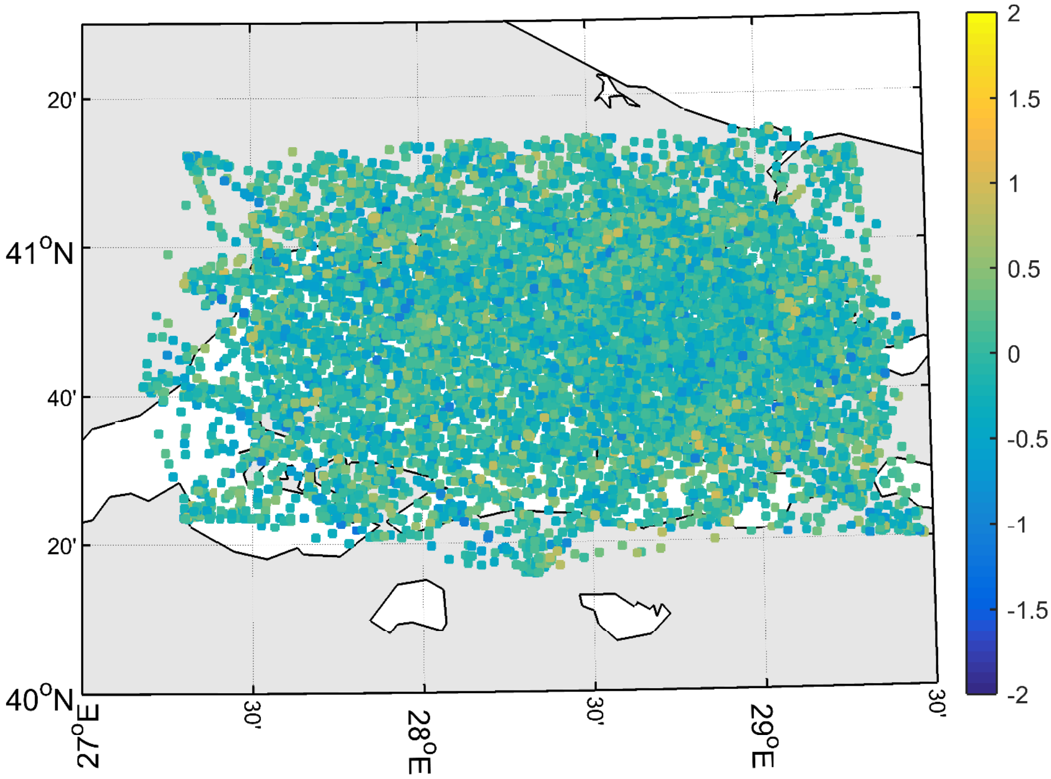

Figure 6: Map of path residuals. Residual is plotted at a random distance between epicentre and station. Because each event-path-site is only sampled once it is not possible to assess the standard deviation of each residual (unlike for event and site terms).

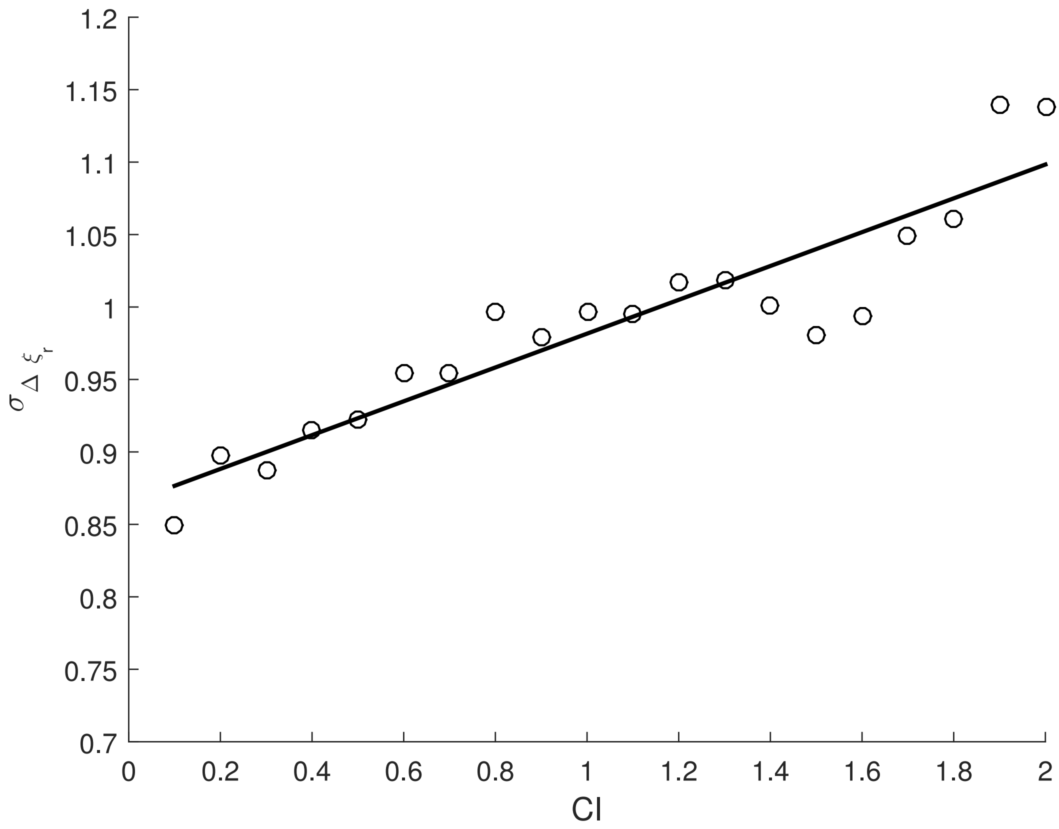

Figure 7: The standard deviation of the normalized residuals ($\sigma_{\Delta\xi_r}$) against closeness index (CI). The equation of the line of best-fit is: $\sigma_{\Delta\xi_r} = 0.8649 + 0.1167\text{CI}$.

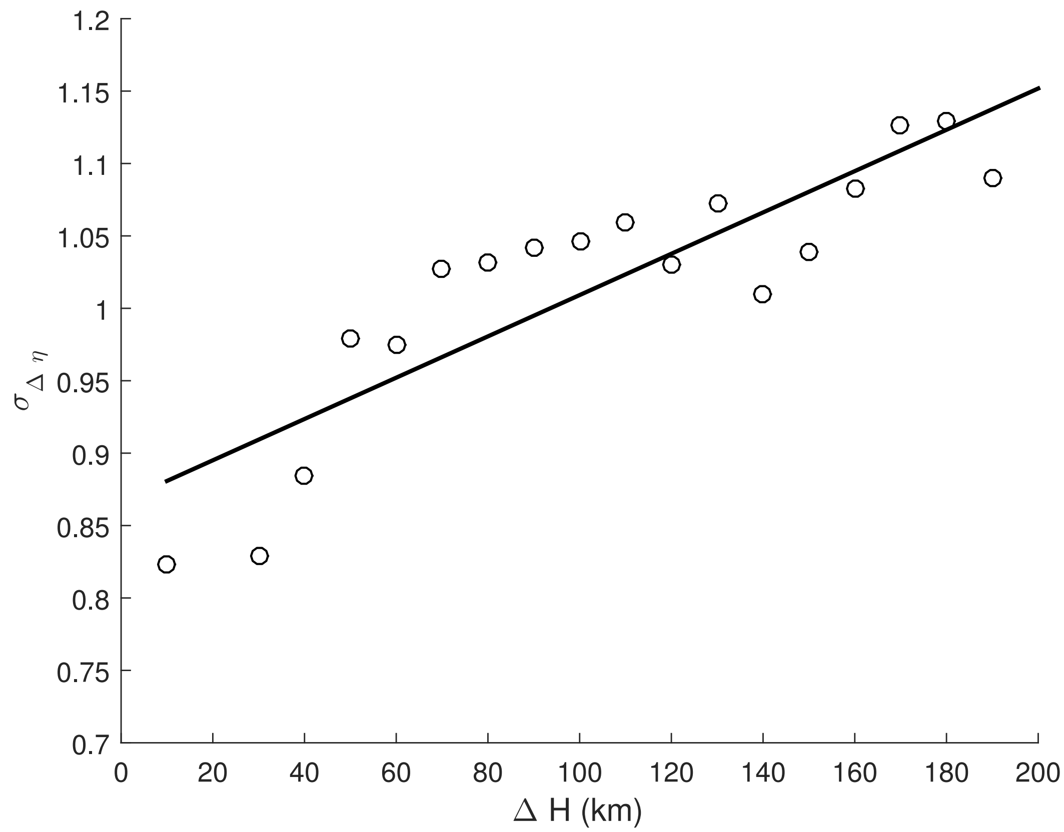

Figure 8: The standard deviation of the normalized residuals ($\sigma_{\Delta\eta}$) against separation distance (ΔH). The equation of the line of best-fit is: $\sigma_{\Delta\eta} = 0.8665 + 0.0014\Delta H$.